Available online at BCREC website: https://bcrec.id

Bulletin of Chemical Reaction Engineering & Catalysis, 15 (2) 2020, 390-404

Research Article

Totally-green Fuels *via* CO_2 Hydrogenation

Lorenzo Spadaro[1,2,*], Alessandra Palella[1,*], Francesco Arena[1,2]

[1]*Istituto CNR di Tecnologie Avanzate per l'Energia "Nicola Giordano", Via S. Lucia sopra Contesse n.5, 98126 Messina, Italy.*
[2]*Dipartimento di Ingegneria, Università degli Studi di Messina, Viale F. Stagno D'Alcontres 31, I-98166, Messina, Italy.*

Received: 1st February 2020; Revised: 21st April 2020; Accepted: 23rd April 2020; Available online: 30th July 2020; Published regularly: August 2020

Abstract

Hydrogen is the cleanest energy vector among any fuels, nevertheless, many aspects related to its distribution and storage still raise serious questions concerning costs, infrastructure and safety. On this account, the chemical storage of renewable-hydrogen by conversion into green-fuels, such as: methanol, *via* CO_2 hydrogenation assumes a role of primary importance, also in the light of a cost-to-benefit analysis. Therefore, this paper investigates the effects of chemical composition on the structural properties, surface reactivity and catalytic pathway of ternary CuO-ZnO-CeO_2 systems, shedding light on the structure-activity relationships. Thus, a series of $CuZnCeO_2$ catalysts, at different CuO/CeO_2 ratio (*i.e.* 0.2-1.2) were performed in the CO_2 hydrogenation reactions at 20 bar and 200-300 °C, (GHSV of 4800 STP $L \cdot kg \cdot cat^{-1} \cdot h^{-1}$). Catalysts were characterized by several techniques including X-ray Diffraction (XRD), N_2-physisorption, single-pulse N_2O titrations, X-ray Photoelectron Spectroscopy (XPS), and Temperature-programmed Reduction with H_2 (H_2-TPR). Depending on preparation method, the results clearly diagnostics the occurrence of synergistic structural-electronic effects of cerium oxide on copper activity, with an optimal 0.5 copper-to-cerium content. The rise of CuO loading up to 30% drives to a considerable increase of hydrogenation activity: C2Z1-C catalyst obtains the best catalytic performance, reaching methanol yield value of 12% at 300 °C. Catalyst activity proceeds according to volcano-shaped relationships, in agreement with a dual sites mechanism.

Keywords: Renewable energy; hydrogen-to-liquid-fuels (HTL); carbon dioxide recycling; methanol synthesis and synfuels

How to Cite: Spadaro, L., Palella, A., Arena, F. (2020). Totally-green Fuels *via* CO_2 Hydrogenation. *Bulletin of Chemical Reaction Engineering & Catalysis*, 15(2), 390-404 (doi:10.9767/bcrec.15.2.7168.390-404)

Permalink/DOI: https://doi.org/10.9767/bcrec.15.2.7168.390-404

1. Introduction

Although electric vehicles are the best environmental choice, the high costs and the limited availability of several materials do not allow the total replacement of thermal engines worldwide. Prompted by the need of meeting the rise in the energy demand and at the same time reducing polluting emissions, the industrialized countries are facing new model of development based on the renewable sources and zero emissions technologies adoption [1–3]. Regarding this, hydrogen is the most abundant element in the universe and it is considered a source of large-scale clean energy, which by 2050 could supply al-

* Corresponding Author.
Email: Lorenzo.spadaro@itae.cnr.it (L. Spadaro); alessandra.palella@itae.cnr.it (A. Palella)

most a quarter of Europe's energy needs and allow to maximize business opportunities towards a future of zero emissions. Indeed, the European Union has identified hydrogen as one of the six strategic areas where major interventions and investments are needed, according to joint funding and assistance from the Horizon Europe program [4]. Despite the potential, the building of the infrastructure, for a hydrogen-based economy, negatively affects this technological choice, as demonstrated by the FCH-JU European industrial partnership (Fuel Cells and Hydrogen Joint Undertaking) which is working on it since 2008, managing more than 250 projects financed with 2 billion euro by public-private funds. In particular, many aspects related to distribution and storage of hydrogen (*i.e.* H_2 highly compressed; 300 bar) still raise serious issues concerning infrastructure and safety. Therefore, to achieve the climate objectives, green-hydrogen from renewable energy sources (*i.e.* wind and sun) is now produced, obtaining new advanced synfuels at low carbon energy for powering hybrid and bi-fuel vehicles, as the most suitable route in the decarbonisation process and eco-life [5–7]. In fact, hydrogen has the double advantage to be a fuel, immediately available for using, and an energy vector, whose chemical accumulation can be pursued through its combination with other molecules.

Furthermore, more than 3 Gton of CO_2 are currently emitted to the atmosphere every month, with tremendous impact on climate change and global warming of the Earth. For this reason, efforts must be put forth to decrease emissions, permanently sequester CO_2 and convert it into valuable products [8–10]. In the light of a cost-to-benefit analysis, the combination of green-hydrogen with CO_2 from industrial processes can assume a key role in the perspective of a more efficient and cleaner energy generation [11–13].

Actually, the application of green-fuels of second-generation is one of the most suitable route to reach industrial and ecological targets in the short term, because of the lower costs, easy commercial adoption and fully industrial development. Differently from fossil, a totally-green fuel does not give rise to extra CO_2 emission in atmosphere, because its combustion, in the well-to-wheel cycle, generates a CO_2 release equal to that necessary for its manufacturing, closing the CO_2 balance, on the other words a fuel at zero-charge of carbon dioxide. On the other hand, besides the efforts to limit the presence of CO_2 in the atmosphere by CCUS technologies, CO_2 is assuming an even more important and strategic play-role in the energy field, as well as in the synthesis of industrial relevant products and chemicals [8,9,14–21]. As new raw material, the direct utilization of CO_2 for industrial purposes finds commercial applications in the synthesis of methanol and other chemical compounds such as olefins and aromatics, which are a rapidly growing field, since CO_2 represents an abundant and economic carbon source [10,22,23]. As one of the most worldwide relevant topics, the work would also reflect on the practical use of the hydrogenation catalysts in combination to economically useful CCUS technologies. Indeed, the catalytic conversion of CO_2 coming from the atmosphere into fuels and fine chemicals would be one of the most profitable and practical solutions to the problem of greenhouse gas emissions, provided that capture/sequestration and high pressure storage technologies are made economically available [8].

Nevertheless, in the very short period, the most prosecutable actions and promising prospective look upon the use of CO_2-rich streams, coming from the industrial exhausted emissions, such as: of brick and cement work, although needs of clean-up stages, and further purification and concentration [16]. On this address, Haldor-Topsoe is at the forefront in the use of CO_2 as carbon feedstock through different power-to-gas technologies, while ENI is redesigning its lines of production in a greener vision, by the development of new hydrogenation processes, called ENI Ecofining™, for the green-fuels synthesis, strategically prefiguring the production of ultra-pure CO_2 as industrial practice [13,24]. Despite considerable progresses made in the science of fuel, the industrial economic feasibility of hydrogen-to-liquid-fuels (HTL), such as: methanol, is still under debate. In this scenario, the development of more efficient catalytic materials for an effective hydrogenation of CO_2 appears of great interest [25–28].

As known, CuO/ZnO-based catalysts have the advantages of lower cost and higher chemical stability compared with other catalysts, such as those based on transition metal carbides (TMCs), bimetallic catalysts or Au-supported catalysts [29,30]. Although $CuO/ZnO/Al_2O_3$ is the most intensively studied catalyst for the methanol synthesis, the use of ZrO_2, CeO_2 and TiO_2 oxides was found to improve both the activity and selectivity of CuO/ZnO-based catalysts in the CO_2 hydrogenation processes. Indeed, Si *et al.* recently

discussed on the influence of replacing Al_2O_3 with CeO_2 in the typical Cu-ZnO/Al_2O_3 catalytic composition for syngas conversion, suggesting that the use of cerium oxide led to a remarkable positive effect on the catalyst stability, as a result of the preservation the ratio of Cu^0/Cu^+ on catalyst surface, as well as on the particle growth, due to the strong electron interactions of the copper/ceria phase ($Cu/Cu_2O/CuO$, Ce^{3+}/Ce^{4+}) during hydrogenation reactions [31]. Metal dispersion and CO_2 adsorption capacity are two key parameters affecting CO_2 hydrogenation functionality of Cu-based systems [32]. Similarly, in our previous works, we displayed that the use of several oxides (*i.e.* as ZnO, ZrO_2, CeO_2, Al_2O_3, Gd_2O_3, Ce_2O_3, Y_2O_3) and alkaline metals (*i.e.* Li, Cs, K) could remarkably influence both catalyst structure and morphology, balancing the amount of the diverse copper species (*i.e.* $Cu°/Cu^+/Cu^{2+}$) and leading to a notable improvement of the catalytic performance [14,15,17,20,33,34]. On this account, ZrO_2 has been shown to positively affect morphology and texture of Cu-ZnO based catalysts, favoring also CO_2 adsorption / activation and methanol selectivity, while CeO_2 could act as both electronic promoter and improver of surface functionality of Cu phase. As reported in our preliminary works, we have proved a greater specific activity of CuZnO-CeO_2 catalyst with respect to that of similar catalytic systems containing ZrO_2 or other promoter oxides, facing several electronic and structural effects [14,15,18]. In spite of a generally higher specific activity, we have evidenced that CuZnO-Ceria catalyst suffers from several practical limitations, such as: a lower surface area, especially compared to that of ZrO_2 and Al_2O_3 promoted catalysts. In particular, we have showed the effects of replacing ZrO_2 carrier with CeO_2 oxide, especially on the development of the surface area of CuZnO-based catalysts. Indeed, by fixing the amount of carrier phase (*i.e.* around 40%), the catalysts without Ceria or at the less content of Ceria obtained a larger MSA and SA exposure and, consequently, a higher CO_2 conversion, despite the minor value of methanol yield per surface area [15,18].

In agreement with the formation of carbonates intermediates induced by the oxygen vacancies related to CeO_2, we have observed a major selectivity to methanol on CuZnO catalysts promoted by CeO_2 addition with respect to other carrier oxides such as ZrO_2 and Al_2O_3. On this regard, our preliminary findings perfectly agree with recent studies of Wang *et al.* who find a higher methanol selectivity on Cu/CeO_2 catalysts with respect to ZrO_2 supported systems, according to an improved metal dispersion and oxygen vacancies formation induced by the interaction at the Cu/CeO_2 interface [35]. Furthermore, Shi *et al.* gave evidence of an improvement in methanol productivity by TNTs addition on CuO-ZnO-CeO_2 catalysts, as a results of enhanced Cu dispersion and CO_2 uptake [36].

On this account, we think that CeO_x phase can act modifying the red-ox properties of the catalyst and improve the surface chemisorption-activation process of CO_2, which remains, actually, one of the main factors determining the catalytic performance of copper-based catalysts [13]. In particular, the process of chemisorption of CO_2 is affected by several factors such as the presence of basic sites and defects on the surface of the catalytic active elements [12,35]. In regard of this, a systematic study on the influence and effect of CeO_2 content on physical-chemical property of CuZnO-based catalysts and, consequently, on the catalysts behavior into CO_2 hydrogenation processes have not still reported, being almost unclear the role of CeO_2 loading.

Therefore, in this study a series of CuZnO-CeO_2 catalysts, with different CuO/CeO_2 weight ratio (*i.e.* 0.2-1.2) and a constant ZnO loading (ca. 15 wt.%), were prepared and tested in the CO_2 hydrogenation reactions at 20 bar and 200-300 °C, aiming to go insight on the activity and selectivity pathways and to shed light on the structure-activity relationships of $CuZnCeO_2$ catalytic formulations.

2. Materials and Methods

2.1 Catalysts

A series of CuZnO-CeO_2 catalysts, with different CuO/CeO_2 weight ratio (*i.e.* 0.2-1.2) and a constant ZnO loading (ca. 15 wt.%), were prepared by reverse co-precipitation under ultrasounds irradiation route, which represent a synthesis method successfully employed since 2007, even from an initial bench scale of grams up to some kilograms, always proving high reproducibility, accuracy and stability in the synthesis of different Cu-based catalytic materials, as confirmed by our previous studies [17,20,33]. Accordingly, an aqueous solution (ca. 100 mL) of $Cu(NO_3)_2{\cdot}3H_2O$ (Sigma-Aldrich, assay 99-104%), $Zn(NO_3)_2{\cdot}6H_2O$ (Sigma-Aldrich, assay ≥99.0%) and $(NH_4)_2Ce(NO_3)_6$ (Sigma-Aldrich, assay ≥98.5%) precursors was added drop-wise to a 1 M $KHCO_3$ (Sigma-Aldrich, assay 99.7%) solution (500 mL) under vigorous stirring and ultrasound irradiation, keeping pH constant at 8.0 by addition of 1M

$KHCO_3$ solution. After precipitation, the solid was kept for 30 minutes under stirring and ultrasounds irradiation. Then, the solid was aged at 30 °C for 2 h, filtered and washed with hot distilled water. Thereafter, the catalysts were dried at 130 °C overnight and further calcined in air at 400 °C for 4 h. After preparation, all catalysts were doped with potassium solution by impregnation for achieving 1.0 wt.% of K_2O. Powdered catalysts were pressed (10 ton·cm^{-2}) and then crushed and sieved to the particle size fraction (16-20 mesh) used for both characterization and testing measurements. Then, in order to further assess the accuracy and preciseness of both synthesis procedure and analytical methods, each batch of prepared catalyst (ca. 500 g each) was studied in double blind tests. Table 1 shows the list of catalysts, also reporting the chemical-physical properties.

2.2 Catalyst Characterization

Surface area (SA), pore volume (PV), and average pore diameter (APD) were obtained from nitrogen adsorption / desorption isotherms (77 K), using a fully automated gas adsorption device (ASAP 2020, Micromeritics Instrument). Physical adsorption isotherms were elaborated by standard BET and BJH methods for SA and PV evaluation, respectively. Before measurements, the samples were out-gassed at 150 °C under vacuum (2 h).

Temperature Programmed Reduction (TPR) analysis was carried out to settle a proper catalyst activation protocol. The TPR measurements were performed in the range 25-700 °C by the use of a semi-automatized laboratory micro-plant equipped with a linear quartz microreactor (i.d. 4 mm) fed with a 5% H_2/Ar mixture flowing at 60 *stp* cm^3·min^{-1} and heated at the rate of 10 °C·min^{-1}. The H_2 consumption was monitored through a Thermal-Conductivity Detector (TCD), calibrated with CuO standard. Under such conditions, TPR was reliable and accurate in terms of both peak position (±5 °C) and hydrogen consumption (±5 %).

Metal Surface Area (MSA) values of catalysts were obtained in the same apparatus by single-pulse N_2O titrations, assuming a Cu:N_2O=2 titration stoichiometry [37]. MSA values were calculated according to procedure elsewhere described [17]. Before measurements, catalysts were reduced in-situ for 1 h at 400 °C under H_2 flow. After reduction, the samples were flushed in the He carrier flow at 410 °C for 15 min, and then cooled to 90 °C for the measurement.

X-ray Diffraction analysis (XRD) of powder samples in the 2θ range of 5-80° were performed by a Philips X-Pert diffractometer operating with Ni β-filtered Cu-Kα radiation at 40 kV and 30 mA, at a scan rate of 0.5°·min^{-1} [14,17]. X-ray fluorescence analysis (XRF) of catalyst was performed with a S8-Tiger WDXRF spectrometer (Bruker-AXS). To calculate the chemical composition of catalysts, Kα1 core-emissions of all chemical elements were taken for the quantitative analysis. The X-ray Photoelectron Spectroscopy (XPS) of samples was performed to value the chemical composition of the catalysts surface. Spectra and quantitative data were obtained using a spectrometer (GMBH PHI 5800-01, Physical Electronics) operating with a monochromatized Al-Kα radiation with a power beam of 300 W. The pass energy for the analysis of concentration and oxidation state of the surface atoms was 58 and 11 eV, respectively. The BE regions of C1s (280-300 eV), Cu2p (920-968 eV), Zn2p (1010-1060 eV), Ce3d (870-935 eV), and O1s (525-535 eV) were investigated, taking the C1s line (284.8 eV) of adventitious carbon as reference [33,34,38–42].

2.3 Catalytic Activity Measurements

Catalytic performance tests were performed at 20 bar and between 200 °C and 300 °C of temperature, using a semiautomatic laboratory micro-plant equipped with a AISI 316 stainless steel Plug Flow Reactor (i.d. 10 mm; e.d. 12 mm; length of 250 mm), loaded with 0.5 g of

Table 1. Chemical-physical properties of $CuZnCeO_2$ catalytic systems (BET Surface Area ($S.A._{BET}$), Average Pore Diameter (A.P.D.) and Pore Volume (P.V.) determined by N_2-physisorption analysis, Metal Surface Area (M.S.A.) determined by single-pulse N_2O titrations).

	Chemical composition (wt.%)				$S.A._{BET}$	M.S.A.	APD	P.V.
	CuO	ZnO	CeO_2	K_2O	$m^2 \cdot g_{cat}^{-1}$	$m^2 \cdot g_{cat}^{-1}$	nm	$cm^3 \cdot g_{cat}^{-1}$
C1Z1C	15.1	14.8	70.1	1.0	126.2	23.9	18	0.33
C2Z1C	29.7	14.7	55.6	0.9	181.0	45.1	17	0.39
C3Z1C	45.8	15.1	39.7	1.0	129.1	40.0	19	0.35

catalyst diluted with 1.0 g of SiC. Before all tests, catalysts were in-situ activated at 400 °C in reducing atmosphere, flowing 5% H_2/Ar gas mixture for 1 h at a heating rate of 10°C·min^{-1}. After catalyst activation, the reactor was fed with a $CO_2/H_2/N_2$ (3/9/1) mixture flowing at 40 *stp* cm^3·min^{-1} (GHSV of 4800 STP L·kg$_{cat}^{-1}$·h^{-1}), using nitrogen as internal standard. Reagents and products were online monitored employing a gas-chromatograph (GC) HP 6890, equipped with a thermal-conductivity detector (TCD) and two packed columns (Porapak Q and 5A Molecular Sieve, Sigma-Aldrich) for the analysis of permanent gasses, and a flame ionization detector (FID) coupled with a capillary column (PoraPLOT Q, i.d. 0.53 mm; length of 30 m, Agilent) for the hydrocarbon species quantification. The products distribution was established by GC-FID, according to the relative sensitive factors of each compound, determined by using several standards. Hydrogen and CO_2 conversion values (X_R, %, with R=H_2 or CO_2), esteemed by GC-TCD analysis with both the internal standard (Equation 1) and the mass balance (Equation 2) methods:

$$\chi_R IS(\%) = \frac{Area_{peak\ R,in} - \left(Area_{peak\ R,out} \times \frac{Area_{peak\ standard,in}}{Area_{peak\ standard,out}} \right)}{Area_{peak\ R,in}} \times 100 \quad (1)$$

$$\chi_R MS(\%) = \frac{Area_{peak\ R,out}}{Area_{peak\ products,out} - Area_{peak\ R,out}} \times 100 \quad (2)$$

where ($Area_{peakstandard,in}/Area_{peakstandard,out}$) is introduced in Equation 1 to normalize the response of the analyte (*i.e.* H_2 or CO_2) to the response of the internal standard (*i.e.* N_2), improving the accuracy of quantitative GC-TCD analysis, as proved by good agreement between IS and MS methods (±5 %) and a reproducibility better than 95%. Meanwhile, selectivity of product *i* (S_i, %) was calculated by GC-FID analysis, according to the following formula (Equation 3):

$$S_i(\%) = \frac{Area_{peak\ product-i}}{\sum Area_{peak\ products,out}} \times 100 \quad (3)$$

According to the use of both IS and MS calculation method, reaching the steady state condition, the reported value of selectivity agrees with that valued on the basis of the amount of formed *i* product with respect to the converted hydrogen (± 2%), as further proof of the accuracy of the analytical method.

The absence of diffusional resistance and the kinetic regime of the catalytic measurements were proved according to the Weisz–Prater ($N_{W-P} < 1.0$) criterion, verifying N_{W-P} values on the order of $10^{-4} - 10^{-5}$, (Equation 4):

$$N_{W-P} = \frac{r_{app}\left(mol \cdot s^{-1} \cdot g_{CAT}^{-1}\right) \cdot \rho_p\left(g \cdot cm^{-3}\right) \cdot \left(d_p/2\right)^2 \left(cm^2\right)}{D_{eff}\left(cm^2 \cdot s^{-1}\right) \cdot C_{H_2S}\left(mol \cdot cm^{-3}\right)} < 1.0 \quad (4)$$

3. Results and Discussion

3.1 Structure and Physical-chemical Properties

Reflecting the synthesis of the catalysts with a different formulation, the chemical analysis of the bulk agrees with the expected composition, proving the effectiveness of the preparation method, which also allows obtaining *meso*-pore structures with enhanced textural properties. Indeed, the catalysts exhibit total surface area (SA) which ranges from 126 to 181 m^2·g$_{cat}^{-1}$ with a similar average pore diameter (APD) of 16-18 nm (Table 1). Then, according to catalyst formulation, the SA has a parabolic tendency with the copper-to-cerium ratio, reaching the greatest extension at the middle CuO content (*i.e.* C2Z1-C catalyst), with the most favorable 0.5 copper-to-cerium ratio. Not depending on preparation method, the similar SA value of C1Z1-C (126 m^2·g$_{cat}^{-1}$) and C3Z1-C (129 m^2·g$_{cat}^{-1}$) catalysts clearly diagnostics the occurrence of a synergistic structural effect between cerium and copper oxides (Table 1).

Apart from minor differences, the XRD analysis reveals that all catalysts are characterized by very similar diffraction patterns, showing a prevalently crystalline catalyst architecture (Figure 1). According to the chemical composition, the XRD patterns of all systems

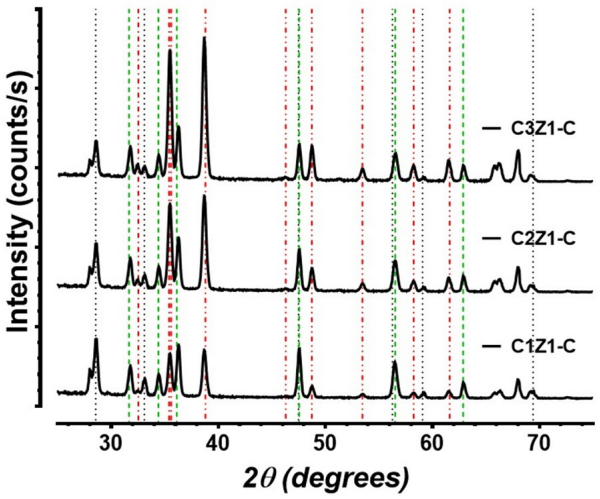

Figure 1. XRD patterns of $CuZnCeO_2$ systems (CeO_2, JCPDS 34-0394 dotted black line; CuO, JCPDS 5-661, dash-dotted line red line; ZnO, JCPDS 08-7114, dashed green line).

consist in the overlapping of the diffraction signals of the crystalline phase of cubic *cerianite* (CeO_2; JCPDS 34-0394), hexagonal *tenorite* (CuO; JCPDS 5-661) and monoclinic *zincite* (ZnO; JCPDS 08-7114) (Figure 1).

Then, TPR analysis proves similar reduction behavior (Figure 2). In fact, the reduction pattern of all catalysts is characterized by two reaction zones, placed at low (LT; 100-270 °C) and high (HT; 300-670 °C) temperature, due to copper (Equations 5-8) and surface ceria (Equation 9) reduction, respectively.

Reduction of ionic dispersed Cu species and/or of coordinative-unsaturated species (CUS):

$$CuO_x + xH_2 \rightarrow Cu° + xH_2O \quad (5)$$

Reduction of isolated copper oxides:

$$2CuO + H_2 \rightarrow Cu_2O + H_2O \quad (6)$$

$$Cu_2O + H_2 \rightarrow 2Cu° + H_2O \quad (7)$$

Reduction of copper in strong interaction with ZnO and CeO_2 phase:

$$CuO\text{-}MO + H_2 \rightarrow Cu° + H_2O \quad (8)$$

Reduction of the ceria surface:

$$2CeO_2 + H_2 \rightarrow Ce_2O_3 + H_2O \quad (9)$$

In particular, the reduction of Cu oxides occurs at temperatures below 290 °C, which is typical of bulk CuO [17], agreeing with the reduction of ionic dispersed copper and CUS (t_{range} of 150-180 °C), isolated CuO and copper clusters in strong interaction with ceria (t_{range} of 200-220 °C) [14,17,33], as shown in Figure 2. In addition, the TPR profile of C1Z1-C catalyst in the LT range reports the presence of an asymmetric peak with a T_{M1} maximum at ca. 210 °C and a shoulder at 190 °C, while the reduction pattern of the high CuO loading catalysts results in two better resolved peaks. Indeed, with equivalent area, the TPR profile of C2Z1-C catalyst revels two convoluted peaks with maxima at 180 °C and 215 °C, respectively. Then, C3Z1-Csample shows a growth of the reduction component at lower temperature, with a peak maximum centered at 178 °C, mirroring an increase of isolated CuO phase, as a consequence of higher loading and minor Cu dispersion [14,17].

The chemical analysis of catalyst surface (ESCA) revels an evident enrichment of Cu and Ce atoms at the surface of the catalyst with respect to the bulk (Figure 3), highlighting the elevate grade of dispersion reached by Cu and Ce species on the catalyst surface through the preparation method [14,15]. In addition, the higher surface concentration of Cu and Ce ions compared to Zn, prefigures the encapsulation of the ZnO phase into a $CuO\text{-}CeO_2$ matrix, also justifying a remarkable chemical affinity between copper and cerium oxide species [18,43,44].

Then, Figure 4 displays the core level spectra of O1s, Cu2p, Zn2p and Ce3d atoms. Apart from minor differences, all catalysts display similar features. Namely, Cu_{2p} spectra display $2p_{1/2}$ (933.0-934.3eV), $2p_{3/2}$ (953.0-953.4 eV)

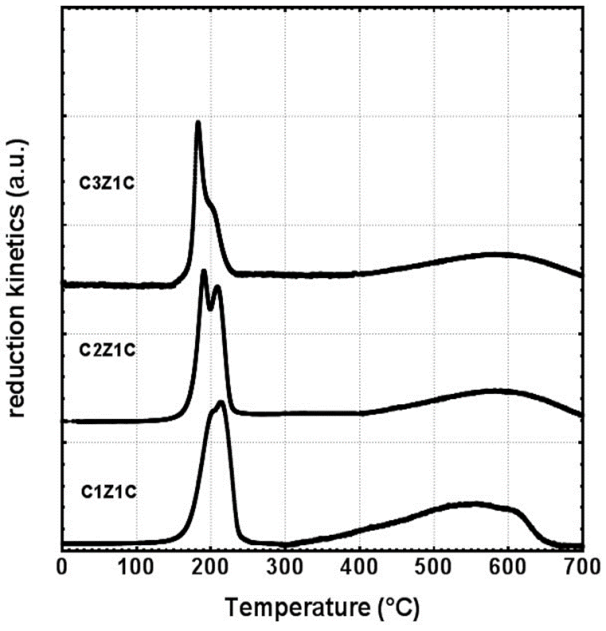

Figure 2. TPR analysis of $CuZnCeO_2$ systems.

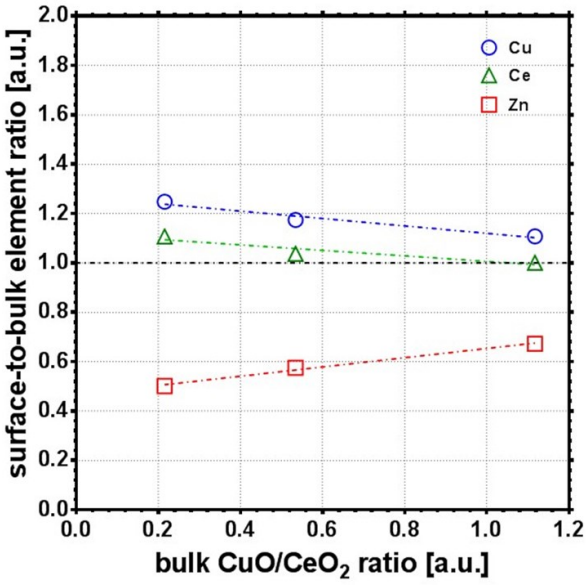

Figure 3. Element surface abundance versus bulk chemical composition.

transitions, and shake-up lines characteristic of oxidized copper [45–47]. According to a higher binding energy of $Cu2p_{3/2}$ (934.3 eV) and O1s (531.3 eV), Cu on the surface of C2Z1-C catalyst prefigures a higher oxidation state, as further confirmed by the evident asymmetry of O1s peak, pointing out the existence of different oxide species [45]. Indeed, the shape of O1s spectra is diagnostic of the presence of various kinds of oxygen species. In particular, the deconvolution analysis well distinguishes the presence of two O1s peaks centered at about 529.9eV (O_I) and 531.6eV (O_{II}), according to *Gaussian-Lorentzian* convolution shape (after *Shirley*-background subtraction), accounting for lattice oxygen (O_I) and molecular oxygen (weakly bonded) and/or adsorbed species such as carbonate and hydroxyl groups (O_{II}) [48–54], as summarized in Table 2. Furthermore, the higher energy position of O1s peaks of C2Z1-C catalyst also prefigures electronic effects of the surrounding ions affecting the electron density, perhaps due to incorporation of Cu^{n+} ions into ceria lattice (*i.e.* solid solutions). Therefore, Zn2p spectra does not reveal any significant difference in term of binding energy. In turn,

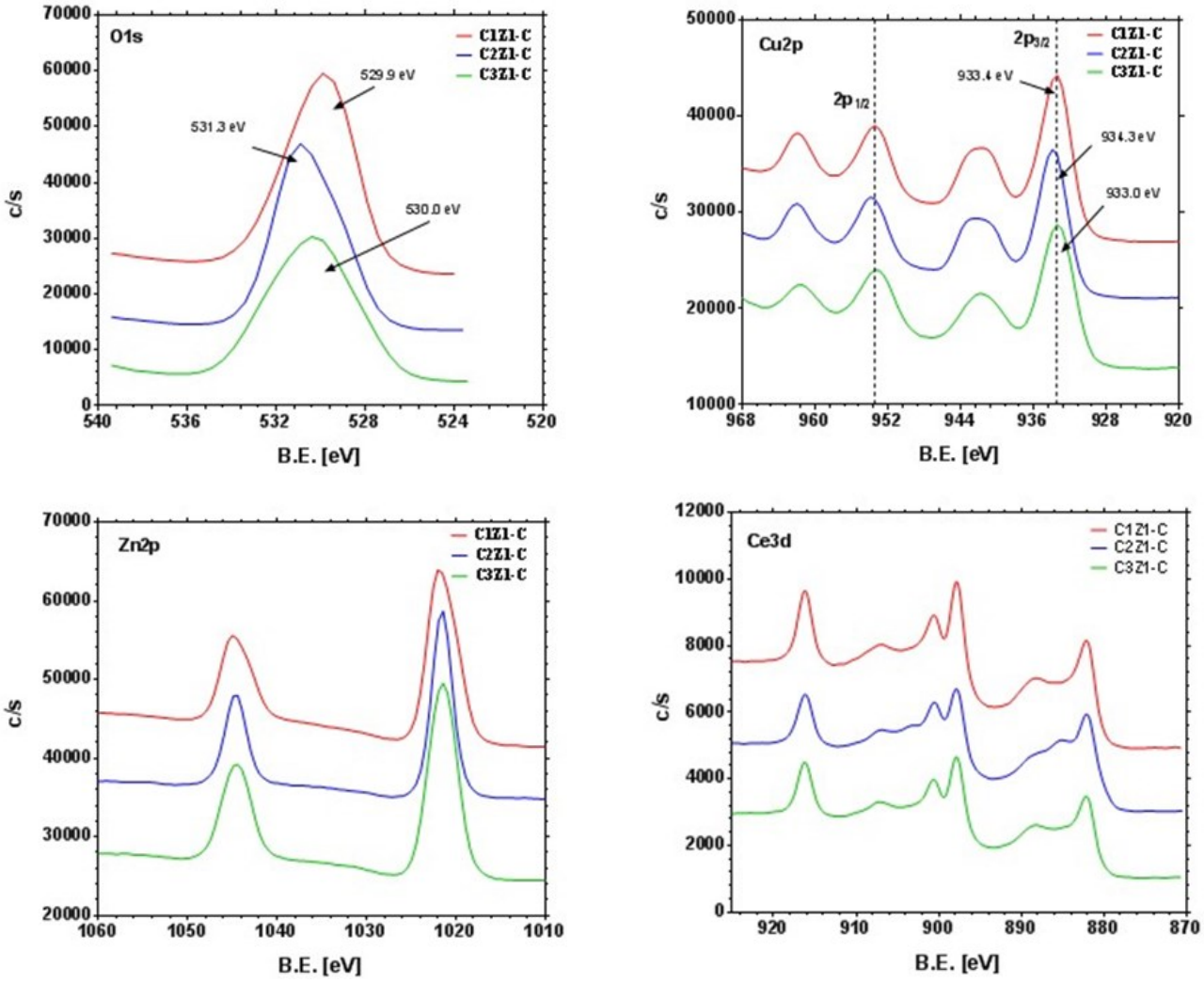

Figure 4. XPS spectra of O1s, Cu2p, Zn 2p and Ce3d core-level transitions.

Table 2. Data of deconvolution analysis of O1s spectra of samples.

	O_{II}		O_{Ia}		O_{II}/O_I+O_{II}
	energy (eV)	area (%)	energy (eV)	area (%)	(--)
C1Z1-C	531.6	27.9	529.8	72.1	0.28
C2Z1-C	531.6	60.4	529.9	39.6	0.60
C3Z1-C	531.6	25.8	529.8	74.2	0.26

the spectra of Ce3d is rather complex due to the evident contribution of six transitions relative to Ce^{4+} and four hidden components of Ce^{3+} ions [40,55,56]. Taking the energy-transition at 916.3 eV as characteristic of Ce^{4+} [40,57], the XPS analysis signals a rise of the Average Oxidation Number (AON) of cerium from 3.5 (*i.e.* C2Z1-C) to 3.8-3.9 (*i.e.* C1Z1-C and C3Z1-C, respectively), as proof of the greater content of Ce^{3+} ions on the surface of C2Z1-C catalyst (Figure 4).

3.2 Results of the Catalytic Tests

The results of catalytic tests in the CO_2 hydrogenation are summarized in Figure 5A-C and in Table 3 in terms of H_2 and CO_2 conversion ($X_{H2/CO2}$), methanol selectivity (S_{CH3OH}), methanol yield (Y_{CH3OH}) and normalized reaction rate (rate). Denoting a similar catalytic pathway, all systems report a progressive increase of the activity with the rise of reaction temperature from 200 °C to 300 °C. However, higher temperature of reaction significantly favors the formation of CO, leading to a notable drop in the methanol selectivity (Figure 5A-C and Table 3).

Thus, the catalysts performance clearly demonstrates the close relationship between chemical composition and catalytic activity. Indeed, the conversion of hydrogen proceeds according to a volcano shaped trend with the growth of the CuO/CeO_2 ratio, as shown in Figure 5A. Namely, regardless of reaction temperature, the increase of CuO loading in the catalyst from 15% to 30% (associated to a consequent decrement of CeO_2 from ca 56% to 40%), drives to a considerable increase of hydrogenation activity at any temperature. Nevertheless, above the 30% of CuO the conversion of hydro-

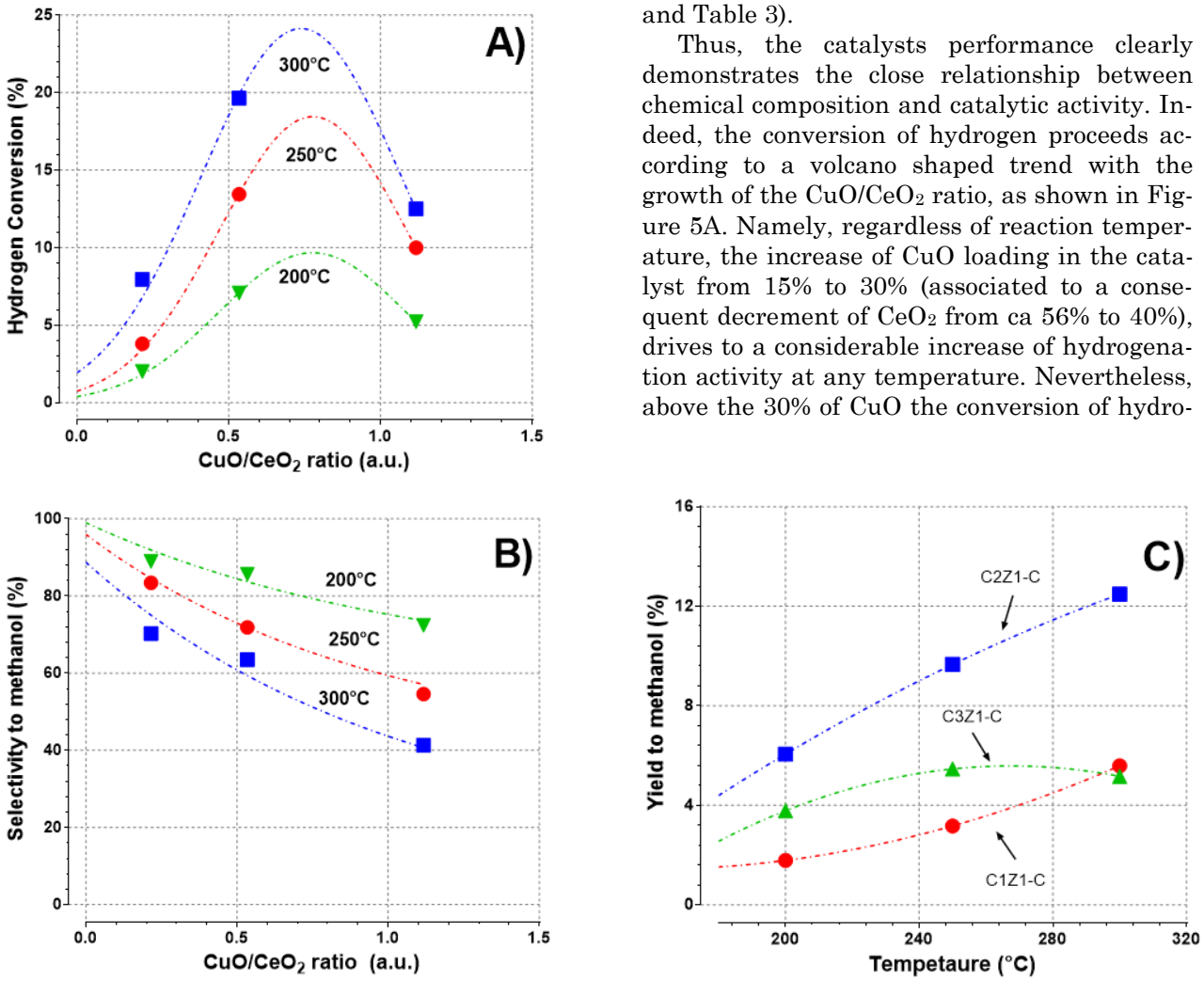

Figure 5. Catalytic results: (A) Conversion of hydrogen (X_{H2}, %), (B) Selectivity to methanol ($S_{methanol}$, %), and (C) Yield to methanol ($Y_{methanol}$, %) at diverse temperature.

Table 3. Catalysts behavior at diverse temperatures: hydrogen and CO_2 conversion ($X_{H2/CO2}$, %), methanol selectivity (S_{CH3OH}, %), and normalized reaction rate (rate, $\mu mol_{(H2)} \cdot g_{cat}^{-1} \cdot s^{-1}$).

	200 °C				250 °C				300 °C			
	X_{H2}	X_{CO2}	S_{CH3OH}	rate	X_{H2}	X_{CO2}	S_{CH3OH}	rate	X_{H2}	X_{CO2}	S_{CH3OH}	rate
C1Z1-C	2.01	2.45	88.96	0.82	3.8	5.06	83.44	1.56	7.95	12.68	70.27	3.26
C2Z1-C	7.07	9.1	85.64	2.9	13.44	21.19	71.88	5.52	19.65	34.11	63.5	8.07
C3Z1-C	5.22	8.13	72.42	2.14	10	19.08	54.6	4.1	12.5	27.16	41.32	5.13

gen slowly goes down (Figure 5A) due to the loss of dispersion, as proved by decreasing of MSA and SA with the Cu loading. Indeed, the MSA_{Cu}-to-Cu ratio decreases from ca. 2.0 of C1Z1-C and C2Z2-C catalyst to 1.0 of C3Z1-C sample, who also shows a surface concentration of Cu comparable to that of bulk, Figure 3. Then, the selectivity to methanol follows an almost exponential decay with the rise of the CuO/CeO_2 ratio, pointing out a greater promoting effect towards the Reverse Water Gas Shift (RWGS) reaction, also favored by the increase of temperature (Figure 5B).

As result of the enhanced structural and chemical properties, C2Z1-C catalyst obtains the best catalytic performance at any temperature, reaching the highest methanol yield value at 300 °C (more than 12%, Figure 5C). Despite of the lesser activity, C3Z1-C catalyst displays a catalytic behavior not so far from that of C2Z1-C sample. In particular, this system shows a progressive rise of methanol formation with temperature up to 250 °C (5.5% of yield), followed by a slight decrease in the methanol synthesis performance consequent with the increasing temperature (5.2% of yield at 300 °C), reflecting the drop in the methanol selectivity (Figure 5C). Then, mirroring the lowest content of active phase (Table 1), methanol yield grows almost exponentially with the rise of temperature on C1Z1-C catalyst, reaching 5.6% at 300 °C, according to the higher selectivity.

Therefore, Table 4 compares the performances of C1Z1-C, C2Z1-C and C3Z1-C catalysts with those other Cu-CeO_2 based catalysts reported in the literature, at similar reaction conditions [23,36,45,58,59], although, the influence of the loading of active CuO elements on the catalytic properties and structure-activity relationships of $CuZnCeO_2$ ternary systems has not been currently systematically analyzed.

The values of methanol productivity reported are comparable, if not superior, with those referred to in the literatures [36,45,59]. In fact, only few works have discussed comparable activity and, when greater than C2Z1-C catalyst (*i.e.* methanol formation rate of 1.40 $\mu mol \cdot g_{cat}^{-1} \cdot s^{-1}$ @ 250 °C and 20 bar), the catalytic performance was almost always referred to catalytic results carried out at higher value of pressure (*i.e.* 30-50 bar), temperature (>250 °C) or H_2-to-CO_2 ratio (>3). In particular, Shi *et al.* [36] recently synthesized a series of CuO-ZnO-CeO_2 and CuO-ZnO-CeO_2/TNTs composite catalysts, attesting an improvement in methanol productivity from 1.39 to 2.64 $\mu mol \cdot g_{cat}^{-1} \cdot s^{-1}$ only after TNTs addition, as improver of Cu dispersion and CO_2 adsorption capacity. Similarly, the lower rate of 1.24 $\mu mol \cdot g_{cat}^{-1} \cdot s^{-1}$ was obtained by Angelo and co-workers at 260 °C and applying very higher pressure (*i.e.* 50 bar) [59] on of CuO-ZnO-CeO_2 based catalysts prepared by conventional co-precipitation. An improvement of productivities were reached when ZrO_2 and Al_2O_3 were introduced in the catalytic formulation in combination with ceria, further evidencing that an optimal balance between the various oxides is a key factor for obtaining materials with enhanced chemical and catalytic properties [23,59]. Thus, the synthesis of methanol and hydrocarbons proceeds through CO_2 activation, which runs with CO_2 chemisorption on catalyst surface, representing a crucial issue of the process. Despite CO_2 is a kinetically stable molecule, the chemisorption process can be

Table 4. Comparison of the performance of Cu-CeO_2-based catalysts in the CO_2 hydrogenation to methanol.

Catalyst	rate ($\mu mol_{CH3OH}/g_{cat} \cdot s$)	T (°C)	P (bar)	H_2/CO_2	ref.
C1Z1	0.44	250	20	3.0	this work
C2Z1	1.37	250	20	3.0	this work
C3Z1	0.75	250	20	3.0	this work
CuO-ZnO-CeO_2	1.39	260	30	3.0	[36]
CuO-ZnO-CeO_2-TNTs	2.64	260	30	3.0	[36]
CuO-CeO_2-TiO_x	0.13	235	30	3.0	[58]
CuO-ZnO-CeO_2	0.22	240	1	9.0	[45]
CuO-ZnO-CeO_2	1.24	260	50	3.9	[36]
CuO-ZnO-ZrO_2-CeO_2 (40:60)	1.44	260	50	3.9	[59]
CuO-ZnO-ZrO_2-CeO_2 (20:80)	1.94	260	50	3.9	[59]
Cu/AlCeO	3.31	260	30	3.0	[23]
Cu/CeO_2	2.08	260	30	3.0	[23]

improved through several factors, such as: a larger exposure of the surface area, surface defects, and a great presence of basic sites. On this regards, all catalysts were promoted in the alkaline character by K_2O adding (1 wt.%).

3.3 Structure-Activity Relationship of CuO-ZnO -CeO_2 Systems

The results of the physical-chemical analysis prove that a high copper loading leads to the sintering of the catalytic surface, also affecting the morphology of the composite materials. Then, the synergism occurring between the oxides of copper and cerium seems to be the key-factor controlling both physical-chemical properties and catalytic behavior of catalyst. With regard to the structural properties (*i.e.* SA and MSA), this study stresses the existence of an optimal content of copper with respect to cerium, which also affects the catalytic performance of the catalyst. Indeed, the CuO-to-CeO_2 weight ratio of about 0.5 accounts for the optimal chemical composition, according to the highest exposure of the surface of C2Z1-C catalyst (SA = 181 $m^2 \cdot g_{cat}^{-1}$; MSA = 45 $m^2 \cdot g_{cat}^{-1}$, Table 1). Then, the quantitative results of XPS deconvolution analysis clearly give evidence of the fact that the catalysts which achieve the better catalytic performance also diagnostic the larger number of oxygen vacancies (Table 2). Indeed, the higher value of $Area_{(OII)}/Area_{(OI+OII)}$ ratio reported by C2Z1-C catalyst proves the larger extension of oxygen vacancies. In particular, C2Z1-C catalyst shows the highest 0.6 value in term of $Area_{(OII)}/Area_{(OI+OII)}$ ratio, also reflecting the lowest A.O.N. of cerium on the surface.

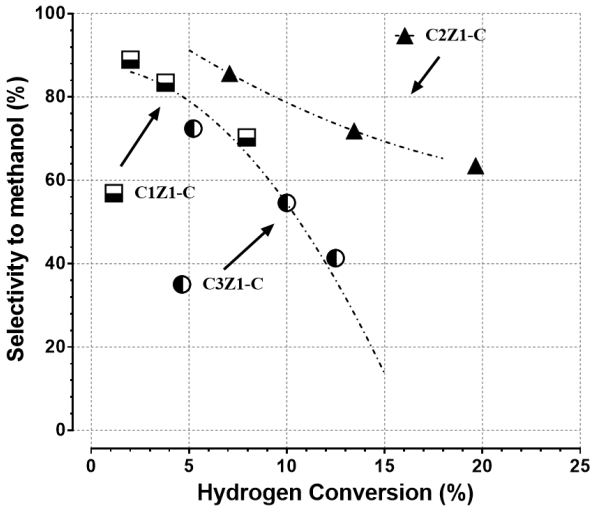

Figure 6. Catalytic results: conversion of hydrogen (%) versus Selectivity to methanol (%).

Independently to CuO content, the progressive increase of H_2 conversion with the increase in temperature is associated to a significant drop in selectivity. From one side, the higher temperature favors the reaction kinetics of hydrogenation and the catalyst activity, prompting methanol synthesis and RWGS reactions. On the other side, the increase of temperature hinders catalyst selectivity to methanol. Because of the opposite effect of temperature, the catalysts report the maximum methanol productivity within 300 °C (Figure 5C). In particular, the best catalytic performance has been achieved by C2Z1-C catalyst at 300 °C, both in term of hydrogenation rate and methanol productivity, reflecting the highest exposure of the catalytic surface and prefiguring the existence of structure-activity relationships. Then, Figure 6 shows the tendency of methanol selectivity as a function of hydrogen conversion. Irrespectively to copper content, C1Z1-C and C3Z1-C catalysts follow an identical reaction profile, as proof of same reaction mechanism occurring on the surface of the two catalysts. Diversely, the trend of C2Z1-C catalyst diverts significantly from that of the other systems, according to a more favorable catalytic pathway, which could prove a different reaction mechanism. Hence, these findings suggest the existence of several factors governing the methanol synthesis, in addition to those strictly related to the hydrogenation functionality of catalyst.

As extensively reported in literature [12,13,60–65], the methanol synthesis via the catalytic CO_2 hydrogenation occurs through different consecutive reactive stages. According to a dual site mechanism, CO_2 is reactively chemisorbed on Cu^+ sites, while H_2 is exclusively chemisorbed on the metallic surface of copper (Cu° sites) and further dissociated. Thus, the chemisorbed CO_2 species and their intermediates are hydrogenated by atomic hydrogen. On this address, the stereochemistry and the chemisorption of the reagents influence the product selectivity. In particular, the CO_2 chemisorbed can assume two different geometries and, among them, the bridge-formate intermediate leads more easily to methanol, also favored by the lower temperature [35,66]. In our previous works [14,15,17,18,20,33,34], we have clarified the role explicated by several promoters as the oxide carriers. In particular, we found that the use of several oxides (*i.e.* as ZnO, ZrO_2, CeO_2, Al_2O_3, Gd_2O_3, Ce_2O_3, Y_2O_3) and alkaline metals (*i.e.* Li, Cs, K) could remarkably influence both catalyst structure and copper AON, balancing of the amount of the di-

verse copper species (*i.e.* Cu°/Cu⁺/Cu²⁺) and leading to a notable improvement of the catalytic performance. In particular, we have demonstrated that ZnO and ZrO_2 act as both structural promoters (favoring the development of the metal surface area and hindering the sintering of Cu° clusters) and electronic promoters (stabilizing the unstable Cu⁺ sites through the formation of oxygen bridges Cu⁺-O-M). Hence, in agreement with the dual site mechanism, we have also shed light on the nature of structure-activity relationships in terms of interfacial area [17,18,20]. The interfacial area represents the contact surface between the Cu° cluster and the oxide phase, reflecting the equilibrium of Cu° and Cu⁺ sites involved in the methanol synthesis. Affecting both the chemisorption process and the catalyst surface coverage, the extension of interfacial area can play a fundamental role in the methanol synthesis [30]. Indeed, irrespectively to the reaction kinetics order, the methanol formation rate is directly proportional to the partial pressure of H_2 and CO_2. Being the concentration of CO_2 and H_2 chemisorbed proportional to the number of active sites, it can be assumed that the reaction rate is directly related to the value of interfacial area, as follows:

$$rate_{CH_3OH} = K \cdot [CO_2]^{\alpha} \cdot [H_2]^{\beta} \propto [Cu^{+}] \cdot [Cu^{\circ}] = f(interfacial\ area)(\alpha\, e\, \beta \neq 0) \quad (10)$$

Hence, an excessive presence of one reagent with respect to the other can be a limit for the reaction kinetics; for instance, a too large exposure of the metallic surface can drive to an excessive hydrogen coverage, which can negatively affect the CO_2 chemisorption and the reaction rate. In addition, the existence of Cu° sites is in direct competition with that of Cu⁺ centers, due to the occurring of both reduction and oxidation process during the catalytic cycle. On this address, the role played by the interfacial area appears even more clear by plotting reaction rate ($\mu mol_{CH3OH} \cdot g_{cat}^{-1} \cdot s^{-1}$) and turn-over-frequency number, esteemed on Cu sites calculated by N_2O titrations (TOF; s^{-1}), as a function of θ parameter (*i.e.* θ = MSA/SA), taken as an index of the extension of the interfacial area [18].

In particular, the reaction rate closely follows the profile of a typical volcano-shaped relationship, with the maximum value reached at about 0.25 θ (*i.e.* C2Z1-C catalyst), as shown in Figure 7A. On this route, the higher catalytic performance of C2Z1-C catalyst would reflect the occurring of a greater synergism between copper and cerium oxides, driving to a more favorable combination of Cu° and Cu⁺ active sites, as well as it would mirror a better structural and electronic effects played by the combination of ZnO and CeO_2 promoters. As further proof of the dual site mechanism, the Fig. 7B shows similar relationships with TOF at the different temperatures. In particular, moving from 200 °C to 300 °C, the peak maximum in TOF shift from θ values of ca. 0.255 to 0.233, reflecting a different kinetic dependence of Cu° and Cu⁺ sites on temperature. In particular, the higher temperature seems to favor catalyst with a greater number of Cu⁺ active sites, which can be explained by the greater energy required for the formation of *bidentate* formate species on Cu⁺ active sites. In addition, catalyst

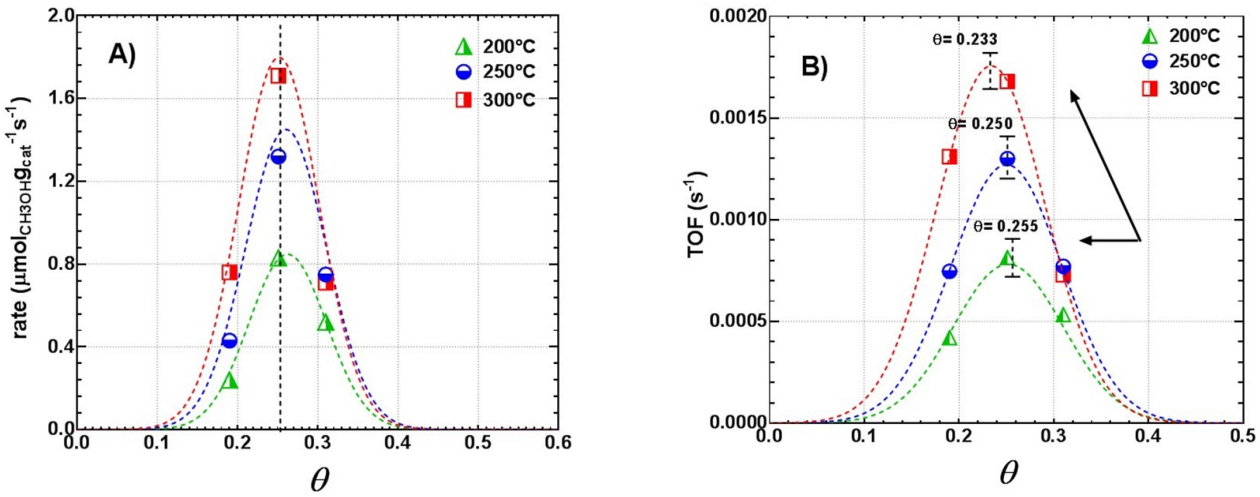

Figure 7. Catalysts structure-activity relationship: (A) normalized reaction rate and (B) TOF versus catalyst interfacial area (θ) at diverse temperature.

reduction and surface dewatering are thermodynamically favored by the higher temperature, while the oxidation processes are disadvantaged by temperature, due to the exothermic nature of the process. On the other hand, a greater reduction of cerium oxide can contribute to stabilize Cu^{+} sites. In addition, the methanol formation might involve highly dispersed Cu ions across the surface and Cu^{0}-O-Cu^{+1} species in interaction with CeO_2 phase, which are strongly hindered by the presence of water on the catalyst surface [16].

4. Conclusions

The influence and effect of CeO_2 content on physical-chemical and catalytic properties into CO_2 hydrogenation processes of $CuZnCeO_2$ catalysts has been assessed. The results diagnostic the occurrence of synergistic structural-electronic effects of cerium oxide on copper activity, with an optimal 0.5 copper-to-cerium ratio. Indeed, C2Z1-C catalyst with CuO-to-CeO_2 ratio of 0.5 reports the highest surface exposure (SA = 181 $m^2 \cdot g_{cat}^{-1}$; MSA = 45 $m^2 \cdot g_{cat}^{-1}$), even obtaining the highest number of oxygen vacancies. As result of the enhanced structural and chemical properties, C2Z1-C catalyst obtains the best catalytic performance at any temperature, reaching the highest methanol yield value of 12% at 300 °C. Therefore, all findings account for a mutual synergistic effect played by CuO-CeO_2 oxides. In particular, the chemical affinity is at the basis of the synergic activity of copper and cerium, reflecting some electronic effects possibly due to incorporation of Cu ions into ceria. The copper-to-cerium ratio is the key-factor controlling physical-chemical properties and catalytic behaviour of catalyst. The conversion of hydrogen proceeds according to a volcano shaped trend with the CuO-to-CeO_2 ratio. Cerium oxide stabilizes Cu^{+} sites, in particular when highly dispersed Cu^{0}-O-Cu^{+1} species interact with CeO_2 phase across interface. As proof of the dual site mechanism of methanol synthesis, the interfacial area extension remarkably affects reaction rates and methanol turn-over-frequency.

Properly, the results obtained in this study assess the practical employment of CuZnO-CeO_2 catalytic compositions in the direct utilization of industrial streams containing CO_2 and in the storage of the surplus of electrical energy through the conversion of H_2 used as chemical-energy vector. This would allow to achieve both the full exploitation of renewable energy resources (*e.g.* wind and solar photovoltaic), through the development of integrated micro-generation energy systems, and the improvement of smart grid systems.

Acknowledgement

Authors are gratefully acknowledged Eco-Rigen S.R.L. for the financial support.

References

[1] IEA. (2018). 2018 World Energy Outlook: Executive Summary. *Oecd/Iea*, 11.

[2] Spadaro, L., Arena, F., Palella, A. (2017). Which Future Route in the Methanol Synthesis? Photocatalytic Reduction of CO_2, the New Challenge in the Solar Energy Exploitation, in *Methanol: Science and Engineering* (eds. Basile, A., and Dalena, F.), Elsevier, pp. 429–472.

[3] Arena, F., Mezzatesta, G., Spadaro, L., Trunfio, G. (2014). Latest Advances in the Catalytic Hydrogenation of Carbon Dioxide to Methanol/Dimethylether, in *Transformation and Utilization of Carbon Dioxide, Green Chemistry and Sustainable Technology* (eds.Bhanage, B.M., and Arai, M.), Berlin Heidelberg, pp. 103–130.

[4] Horizon Europe Program https://www.fch.europa.eu.

[5] Agirre, I., Gandarias, I., Arias, P.L. (2019). Process design and techno-economic analysis of gas and aqueous phase maleic anhydride production from biomass-derived furfural. *Biomass Convers. Biorefinery*, 22. doi: 10.1007/s13399-019-00462-w

[6] Spadaro, L., Palella, A., Frusteri, F., Arena, F. (2015). Valorization of crude bio-oil to sustainable energy vector for applications in cars powering and on-board reformers via catalytic hydrogenation. *Int. J. Hydrogen Energy*, 40(42), 14507–14518.

[7] Schemme, S., Breuer, J.L., Köller, M., Meschede, S., Walman, F., Samsun, R.C., Peters, R., Stolten, D. (2019). H_2-based synthetic fuels: A techno-economic comparison of alcohol, ether and hydrocarbon production. *Int. J. Hydrogen Energy*, 45(8), 5395-5414.

[8] Sanz-Pérez, E.S., Murdock, C.R., Didas, S.A., Jones, C.W. (2016). Direct Capture of CO_2 from Ambient Air. *Chem. Rev.*, 116(19), 11840–11876.

[9] Azarabadi, H., Lackner, K.S. (2019). A sorbent-focused techno-economic analysis of direct air capture. *Appl. Energy*, 250, 959–975.

[10] Ma, Z., Porosoff, M.D. (2019). Development of Tandem Catalysts for CO_2 Hydrogenation to Olefins. *ACS Catal.*, 9(3), 2639–2656.

[11] Allam, D., Cheknoun, S., Hocine, S. (2019). Operating Conditions and Composition Effect on the Hydrogenation of Carbon Dioxide Performed over $CuO/ZnO/Al_2O_3$ Catalysts. *Bull. Chem. React. Eng. Catal.*, 14(3), 604-613. doi: 10.9767/bcrec.14.3.3451.604-613

[12] Olah, G.A., Goeppert, A., Prakash, G.K.S. (2009). Chemical Recycling of Carbon Dioxide to Methanol and Dimethyl Ether: From Greenhouse Gas to Renewable, Environmentally Carbon Neutral Fuels and Synthetic Hydrocarbons. *J. Org. Chem.*, 74(2), 487–498.

[13] Goeppert, A., Czaun, M., Jones, J.P., Surya Prakash, G.K., Olah, G.A. (2014). Recycling of carbon dioxide to methanol and derived products-closing the loop. *Chem. Soc. Rev.*, 43(23), 7995–8048.

[14] Arena, F., Mezzatesta, G., Zafarana, G., Trunfio, G., Frusteri, F., Spadaro, L. (2013). Effects of oxide carriers on surface functionality and process performance of the Cu-ZnO system in the synthesis of methanol via CO_2 hydrogenation. *J. Catal.*, 300, 141–151.

[15] Arena, F., Mezzatesta, G., Zafarana, G., Trunfio, G., Frusteri, F., Spadaro, L. (2013). How oxide carriers control the catalytic functionality of the Cu–ZnO system in the hydrogenation of CO_2 to methanol. *Catal. Today*, 210, 39–46.

[16] Spadaro, L., Arena, F., Negro, P., Palella, A. (2018). Sunfuels from CO_2 exhaust emissions: Insights into the role of photoreactor configuration by the study in laboratory and industrial environment. *J. CO_2 Util.*, 26, 445–453.

[17] Arena, F., Barbera, K., Italiano, G., Bonura, G., Spadaro, L., Frusteri, F. (2007). Synthesis, characterization and activity pattern of Cu–ZnO/ZrO_2 catalysts in the hydrogenation of carbon dioxide to methanol. *J. Catal.*, 249(2), 185–194.

[18] Spadaro, L., Santoro, M., Palella, A., Arena, F. (2017). Hydrogen Utilization in Green Fuel Synthesis via CO_2 Conversion to Methanol over New Cu-Based Catalysts. *ChemEngineering*, 1(2), 19-30.

[19] Sebastián, D., Palella, A., Baglio, V., Spadaro, L., Siracusano, S., Negro, P., Niccoli, F., Aricò, A.S. (2017). CO_2 reduction to alcohols in a polymer electrolyte membrane co-electrolysis cell operating at low potentials. *Electrochim. Acta*, 241, 28–40.

[20] Arena, F., Italiano, G., Barbera, K., Bordiga, S., Bonura, G., Spadaro, L., Frusteri, F. (2008). Solid-state interactions, adsorption sites and functionality of Cu-ZnO/ZrO_2 catalysts in the CO_2 hydrogenation to CH_3OH. *Appl. Catal. A Gen.*, 350(1), 16–23.

[21] Álvarez, A., Bansode, A., Urakawa, A., Bavykina, A. V., Wezendonk, T.A., Makkee, M., Gascon, J., Kapteijn, F. (2017). Challenges in the Greener Production of Formates/Formic Acid, Methanol, and DME by Heterogeneously Catalyzed CO_2 Hydrogenation Processes. *Chem. Rev.*, 117(14), 9804–9838.

[22] Ramirez, A., Dutta Chowdhury, A., Dokania, A., Cnudde, P., Caglayan, M., Yarulina, I., Abou-Hamad, E., Gevers, L., Ould-Chikh, S., De Wispelaere, K., Van Speybroeck, V., Gascon, J. (2019). Effect of Zeolite Topology and Reactor Configuration on the Direct Conversion of CO_2 to Light Olefins and Aromatics. *ACS Catal.*, 9(7), 6320–6334.

[23] Li, S., Guo, L., Ishihara, T. (2020). Hydrogenation of CO_2 to methanol over Cu/AlCeO catalyst. *Catal. Today*, 339, 352–361.

[24] Baldiraghi, F., Stanislao, M. Di, Faraci, G., Perego, C., Marker, T., Gosling, C., Kokayeff, P., Kalnes, T., Marinangeli, R. (2009). Ecofining: New Process for Green Diesel Production from Vegetable Oil, in *Sustainable Industrial Processes* (eds. Cavani, F., Centi, G., Perathoner, S., and Trifirò, F.), Wiley-VCH Varlag Gmbh & Co. KGaA, pp. 427–438.

[25] Wang, G., Mao, D., Guo, X., Yu, J. (2019). Methanol synthesis from CO_2 hydrogenation over CuO-ZnO-ZrO_2-M_xO_y catalysts (M=Cr, Mo and W). *Int. J. Hydrogen Energy*, 44(8), 4197–4207.

[26] Xiao, J., Mao, D., Wang, G., Guo, X., Yu, J. (2019). CO_2 hydrogenation to methanol over CuO-ZnO-TiO_2-ZrO_2 catalyst prepared by a facile solid-state route: The significant influence of assistant complexing agents. *Int. J. Hydrogen Energy*, 44(29), 14831–14841.

[27] Li, F., Zhan, H., Zhao, N., Xiao, F. (2017). CO_2 hydrogenation to methanol over La-Mn-Cu-Zn-O based catalysts derived from perovskite precursors. *Int. J. Hydrogen Energy*, 42(32), 20649–20657.

[28] Tan, Q., Shi, Z., Wu, D. (2018). CO_2 Hydrogenation to Methanol over a Highly Active Cu-Ni/CeO_2-Nanotube Catalyst. *Ind. Eng. Chem. Res.*, 57, 10148–10158.

[29] Chang, K., Wang, T., Chen, J.G. (2019). Methanol Synthesis from CO_2 Hydrogenation over CuZnCeTi Mixed Oxide Catalysts. *Ind. Eng. Chem. Res.*, 58(19), 7922–7928.

[30] Tada, S., Kayamori, S., Honma, T., Kamei, H., Nariyuki, A., Kon, K., Toyao, T., Shimizu, K.I., Satokawa, S. (2018). Design of Interfacial Sites between Cu and Amorphous

ZrO_2 Dedicated to CO_2-to-Methanol Hydrogenation. *ACS Catal.*, 8(9), 7809–7819.

[31] Si, C., Ban, H., Chen, K., Wang, X., Cao, R., Yi, Q., Qin, Z., Shi, L., Li, Z., Cai, W., Li, C. (2020). Insight into the positive effect of Cu0/Cu+ ratio on the stability of Cu-ZnO-CeO_2 catalyst for syngas hydrogenation. *Appl. Catal. A Gen.*, 594, 117466-117475.

[32] Sripada, P., Kimpton, J., Barlow, A., Williams, T., Kandasamy, S., Bhattacharya, S. (2020). Investigating the dynamic structural changes on Cu/CeO_2 catalysts observed during CO_2 hydrogenation. *J. Catal.*, 381, 415–426.

[33] Arena, F., Italiano, G., Barbera, K., Bonura, G., Spadaro, L., Frusteri, F. (2009). Basic evidences for methanol-synthesis catalyst design. *Catal. Today*, 143(1–2), 80–85.

[34] Arena, F., Spadaro, L., Di Blasi, O., Bonura, G., Frusteri, F. (2004). Integrated synthesis of dimethylether via CO_2 hydrogenation, in *Studies in Surface Science and Catalysis*, 147, 385–390.

[35] Wang, W., Qu, Z., Song, L., Fu, Q. (2020). CO_2 hydrogenation to methanol over Cu/CeO_2 and Cu/ZrO_2 catalysts: Tuning methanol selectivity via metal-support interaction. *J. Energy Chem.*, 40, 22–30.

[36] Shi, Z., Tan, Q., Wu, D. (2019). Enhanced CO_2 hydrogenation to methanol over TiO_2 nanotubes-supported CuO-ZnO-CeO_2 catalyst. *Appl. Catal. A Gen.*, 581, 58–66.

[37] Evans, J.W., Wainwright, M.S., Bridgewater, A.J., Young, D.J. (1983). On the determination of copper surface area by reaction with nitrous oxide. *Appl. Catal.*, 7(1), 75–83.

[38] Spadaro, L., Arena, F., Granados, M.L., Ojeda, M., Fierro, J., Frusteri, F. (2005). Metal–support interactions and reactivity of Co/CeO_2 catalysts in the Fischer–Tropsch synthesis reaction. *J. Catal.*, 234(2), 451–462.

[39] Arena, F., Famulari, P., Interdonato, N., Bonura, G., Frusteri, F., Spadaro, L. (2006). Physico-chemical properties and reactivity of Au/CeO_2 catalysts in total and selective oxidation of CO. *Catal. Today*, 116(3), 384–390.

[40] Arena, F., Trunfio, G., Fazio, B., Negro, J., Spadaro, L. (2009). Nanosize effects, physicochemical properties, and catalytic oxidation pattern of the redox-precipitated $MnCeO_x$ system. *J. Phys. Chem. C*, 113(7), 2822–2829.

[41] Fazio, B., Spadaro, L., Trunfio, G., Negro, J., Arena, F. (2011). Raman scattering of MnO_x-CeO_x composite catalysts: Structural aspects and laser-heating effects. *J. Raman Spectrosc.*, 42(7), 1583–1588.

[42] Barbera, K., Frusteri, L., Italiano, G., Spadaro, L., Frusteri, F., Perathoner, S., Centi, G. (2014). Low-temperature graphitization of amorphous carbon nanospheres. *Cuihua Xuebao/Chinese J. Catal.*, 35(6), 869–876.

[43] Zhang, L., Pan, L., Ni, C., Sun, T., Zhao, S., Wang, S., Wang, A., Hu, Y. (2013). CeO_2-ZrO_2-promoted CuO/ZnO catalyst for methanol steam reforming. *Int. J. Hydrogen Energy*, 38(11), 4397–4406.

[44] Zhang, L., Lei, J.-T., Tian, Y., Hu, X., Bai, J., Pan, L.-W., Liu, D., Yang, Y. (2015). Effect of precursor and precipitant concentration on the performance of CuO/ZnO/CeO_2-ZrO_2 catalyst for methanol steam reforming. *Ranliao Huaxue Xuebao/Journal Fuel Chem. Technol.*, 43(11), 1366–1374.

[45] Allam, D., Bennici, S., Limousy, L., Hocine, S. (2019). Improved Cu- and Zn-based catalysts for CO_2 hydrogenation to methanol. *Comptes Rendus Chim.*, 22(2–3), 227–237.

[46] Dong, X., Li, F., Zhao, N., Tan, Y., Wang, J., Xiao, F. (2017). CO_2 hydrogenation to methanol over Cu/Zn/Al/Zr catalysts prepared by liquid reduction. *Cuihua Xuebao/Chinese J. Catal.*, 38(4), 717–725.

[47] Liu, J., Han, C., Yang, X., Gao, G., Shi, Q., Tong, M., Liang, X., Li, C. (2016). Methyl formate synthesis from methanol on titania supported copper catalyst under UV irradiation at ambient condition: Performance and mechanism. *J. Catal.*, 333, 162–170.

[48] Zhang, K., Peng, X., Cao, Y., Yang, H., Wang, X., Zhang, Y., Zheng, Y., Xiao, Y., Jiang, L. (2019). Effect of MnO_2 morphology on its catalytic performance in lean methane combustion. *Mater. Res. Bull.*, 111, 338–341.

[49] Li, J., Li, M., Gui, P., Zheng, L., Liang, J., Xue, G. (2019). Hydrothermal synthesis of sandwich interspersed $LaCO_3OH/Co_3O_4$/graphene oxide composite and the enhanced catalytic performance for methane combustion. *Catal. Today*, 327, 134–142.

[50] Yu, Q., Wang, C., Li, X., Li, Z., Wang, L., Zhang, Q., Wu, G., Li, Z. (2019). Engineering an effective MnO_2 catalyst from $LaMnO_3$ for catalytic methane combustion. *Fuel*, 239, 1240–1245.

[51] Yang, N., Ni, S., Sun, Y., Zhu, Y. (2018). A facial strategy to synthesize Pd/Co_3O_4 nanosheets with enhanced performance for methane catalytic oxidation. *Mol. Catal.*, 452, 28–35.

[52] Zhang, Y., Qin, Z., Wang, G., Zhu, H., Dong, M., Li, S., Wu, Z., Li, Z., Wu, Z., Zhang, J., Hu, T., Fan, W., Wang, J. (2013). Catalytic performance of MnO_x -NiO composite oxide in lean methane combustion at low temperature. *Appl. Catal. B Environ.*, 129, 172–181.

[53] Palella, A., Spadaro, L., Di Chio, R., Arena, F. Effective low-temperature catalytic methane oxidation over Mn-CeO_2 catalytic compositions Alessandra. *Catal. Today*. voll

[54] Wang, X., Liu, Y., Zhang, Y., Zhang, T., Chang, H., Zhang, Y., and Jiang, L. (2018) Structural requirements of manganese oxides for methane oxidation: XAS spectroscopy and transition-state studies. *Appl. Catal. B Environ.*, 229, 52–62.

[55] Arena, F., Di Chio, R., Filiciotto, L., Trunfio, G., Espro, C., Palella, A., Patti, A., Spadaro, L. (2017). Probing the functionality of nanostructured $MnCeO_x$ catalysts in the carbon monoxide oxidation. Part II. Reaction mechanism and kinetic modelling. *Appl. Catal. B Environ.*, 218, 803–809.

[56] Arena, F., Di Chio, R., Fazio, B., Espro, C., Spiccia, L., Palella, A., Spadaro, L. (2017). Probing the functionality of nanostructured $MnCeO_x$ catalysts in the carbon monoxide oxidation. Part I. Influence of cerium addition on structure and CO oxidation activity. *Appl. Catal. B Environ.*, 210, 14–22.

[57] Larachi, F., Pierre, J., Adnot, A., Bernis, A. (2002). Ce3d XPS study of composite $Ce_xMn_{1-x}O_{2-y}$ wet oxidation catalysts. *Appl. Surf. Sci.*, 195, 236–250.

[58] Chang, K., Wang, T., Chen, J.G. (2017). Hydrogenation of CO_2 to methanol over CuCeTiO catalysts. *Appl. Catal. B Environ.*, 206, 704–711.

[59] Angelo, L., Kobl, K., Tejada, L.M.M., Zimmermann, Y., Parkhomenko, K., Roger, A.-C. (2015) Study of $CuZnMO_x$ oxides (M=Al, Zr, Ce, CeZr) for the catalytic hydrogenation of CO_2 into methanol. *Comptes Rendus Chim.*, 18(3), 250–260.

[60] Rhodes, M.D., Bell, A.T. (2005) The effects of zirconia morphology on methanol synthesis from CO and H_2 over Cu/ZrO_2 catalysts: Part I. Steady-state studies. *J. Catal.*, 233, 198–209.

[61] Rhodes, M.D., Pokrovski, K.A., Bell, A.T. (2005) The effects of zirconia morphology on methanol synthesis from CO and H_2 over Cu/ZrO_2 catalysts: Part II. Transient-response infrared studies. *J. Catal.*, 233 (1), 210–220.

[62] Sio, C., Sio, C.Z., Fisher, I.A., Bell, A.T. (1997). In-Situ Infrared Study of Methanol Synthesis from H_2/CO_2. *J. Catal.*, 172, 222–237.

[63] Fisher, I.A., Bell, A.T. (1998). In Situ Infrared Study of Methanol Synthesis from H_2/CO over Cu/SiO_2 and Cu/ZrO_2/SiO_2. *J. Catal.*, 178, 153–173.

[64] Grabow, L.C., Mavrikakis, M. (2011) Mechanism of methanol synthesis on cu through CO_2 and CO hydrogenation. *ACS Catal.*, 1(4), 365–384.

[65] Rasmussen, P.B., Holmblad, P.M., Askgaard, T., Ovesen, C. V., Stoltze, P., Nørskov, J.K., Chorkendorff, I. (1994). Methanol synthesis on Cu(100) from a binary gas mixture of CO_2 and H_2. *Catal. Letters*, 26(3–4), 373–381.

[66] Fisher, I.A., Woo, H.C., Bell, A.T. (1997). Effects of zirconia promotion on the activity of Cu/SiO_2 for methanol synthesis from CO/H_2 and CO_2/H_2. *Catal. Letters*, 44(1–2), 11–17.